Tellus (2004), 56B, 413–425
Printed in UK. All rights reserved

TELLUS

Impact of horizontal spatial resolution on the derivation of the source–receptor relationship—an extra-tropical cyclone case

By JAE-BUM LEE and TAE-YOUNG LEE*, *Laboratory for Atmospheric Modeling Research/Department of Atmospheric Sciences, Yonsei University, Seodaemoon-Ku, Seoul 120-749, Korea*

(Manuscript received 12 January 2004; in final form 10 May 2004)

ABSTRACT

A numerical study has been made to evaluate the impact of horizontal resolution on the estimation of the source–receptor (S–R) relationship. Numerical experiments with four different horizontal grid sizes have been performed for an extra-tropical cyclonic episode in East Asia. CSU RAMS and YU-SADM (Yonsei University's sulfuric acid deposition model) have been used to simulate meteorological and pollutant fields, respectively.

In this study, enhanced spatial resolution has improved the simulation of an extra-tropical cyclone, cold front and associated precipitation systems. As spatial resolution increases, the circulation associated with the cyclone and cold front becomes stronger, and the amount of frontal rainfall increases. This study has shown that enhancement of spatial resolution tends to increase self-contributions but decrease foreign contributions to the wet deposition associated with an extra-tropical cyclone. It has been found that increased precipitation for enhanced spatial resolution reduces the amount of transported pollutant but increases the wet deposition of locally emitted pollutants. The larger self-contribution for higher resolutions may also be partially due to the increased strength of resolved convection. The impact of enhancing spatial resolution on dry deposition is felt mostly over downstream regions where the centres of the lows and fronts pass. Contributions from upstream sources increase as cyclonic circulation becomes stronger with increasing spatial resolution. On the other hand, enhancing spatial resolution does not significantly affect the S–R relationship for either dry or wet deposition in the other regions where the extra-tropical cyclone does not pass. This study indicates that improved simulation of a cold front does not significantly affect the S–R relationship for wet deposition over the area of passage of the cold front. An additional discussion infers a S–R relationship for the wet deposition associated with a typical extra-tropical cyclone.

1. Introduction

Long-range transport of atmospheric pollutant is a very important environmental issue in Eastern Asia where a large quantity of pollutants are being emitted into the air. Contributions from domestic and foreign sources to pollutant deposition in a certain receptor region have been the subject of international interest. Several efforts have been made to derive a source–receptor (S–R) relationship in East Asia (Huang et al. 1995; Ichikawa and Fujita 1995; Arndt et al. 1998; Calori et al. 2001). S–R relationships derived by these studies show significant differences from each other. The model intercomparison study by Carmichael et al. (2002), with identical inputs for meteorology and emission rates, has shown that numerically derived S–R relationship can vary greatly with the model.

A numerically derived S–R relationship may contain large uncertainties, which may constitute a significant portion of its variability. Major sources for the uncertainties may include incomplete parametrizations of subgrid-scale physics and chemistry and input fields for meteorology and emission rates.

Long-term S–R relationships are generally obtained with coarse-grid (e.g. a 50–100 km grid) models, due to the large amount of computation required. Meteorological fields from such a coarse-grid model may have various deficiencies in the strength of circulation and in the representation of mesoscale features that can be important for deposition of pollutants. It is important to know how spatial resolution affects a numerically derived S–R relationship.

An extra-tropical cyclone is a very important agent of wet deposition of transported pollutants in mid-latitude regions. Wet deposition associated with an extra-tropical cyclone occurs mainly in the warm and cold frontal precipitation area. Numerical models can predict the frontal precipitation to some extent. However,

*Corresponding author.
e-mail: lty@atmos.yonsei.ac.kr

predicted precipitation may vary greatly with spatial resolution. In particular, the precipitation associated with the cold front, which has scales of a few to 100 km, is not simulated properly with coarse grids. The strength of simulated circulations associated with the cyclone and front may also vary significantly with spatial resolution. They are often weaker with coarse grids than with finer grids. Thus, the spatial resolution can significantly affect the transport of pollutants and, consequently, S–R relationships for both dry and wet deposition.

In this study, numerical experiments have been carried out to investigate the impact of horizontal spatial resolution on the simulation of an extra-tropical cyclone and the S–R relationship for the dry and wet deposition of pollutants within the simulated extra-tropical cyclone. For this study, an extra-tropical cyclone episode has been considered. Numerical experiments have been carried out with four horizontal grid sizes (120, 60, 20 and 10 km). Methodology and the descriptions of the model and case are provided in Section 2. Section 3 includes (1) a comparison of simulated meteorological fields of different spatial resolution, (2) a description of simulated concentration and deposition, (3) the impact of spatial resolution on the S–R relationship for dry and wet deposition during the entire integration period and (4) the S–R relationship for wet deposition in a typical extra-tropical cyclone. Finally, conclusions are given in Section 4.

2. Methodology

Meteorological fields are simulated using CSU RAMS (Pielke et al. 1992). Transport, conversion and deposition of pollutants are simulated using Yonsei University's sulfur acid deposition model (YU-SADM) using 1-hourly outputs of CSU RAMS. The S–R relationship is obtained using the tagged species method. YU-SADM and the method for calculation of the S–R relationship are described in this section.

2.1. Experimental design

Meteorological fields of four different spatial resolutions are prepared for the numerical experiments: 120, 60, 20 and 10 km grids. Nested grid systems are used to accommodate the increased resolution (e.g. nested grid: 60 km grid for experiment 2 (EXP2) and 60, 20 and 10 km grids for EXP4) for the simulation of meteorology. Initial fields for meteorological simulation are from the global analysis ($1.25^\circ \times 1.25^\circ$) data of the Japan Meteorological Agency. Vertical grids are stretched from 100 m for the lowest grid with a stretch ratio of 1.15. The maximum size of the vertical grid is limited to 1000 m. The top of the model is at 25 km.

Transport and deposition of sulfur are simulated using 1-hourly meteorological fields of different spatial resolution (Table 1). Meteorological fields at each time step are interpolated in time using the 1 h data. The simulations are carried out in the same domain (shown in Fig. 1) for EXPs 1, 2 and 3. The domain for EXP4 (10 km grid experiment) is smaller than the domain shown in Fig. 1 by 100 km for each horizontal side. Since the emission rates in the area near the lateral boundaries are small in general, the effect of this difference in area on the derived S–R relationship is assumed to be small. Emission rates for finer grids have been prepared in the following manner. It is assumed that the emission rate (μg m^{-2} s^{-1}) within a coarse (i.e. 120 km $\times$ 120 km) grid is uniform, so that finer grids within a coarse grid area have the same emission rate as that of the corresponding coarse grid. That is, the amount of pollutant emitted from a given coarse grid area is the same for all experiments.

Source–receptor relationships are calculated from the model results. Nine S–R regions are considered, as shown in Fig. 1. Sulfur emission is assumed to consist of SO_2 (95%) and SO_4 (5%). The emission rate for SO_2 is from Oliver et al. (1996) (EDGAR version 2.0) (Fig. 1), which is for the year 1990. A constant emission rate will also be used for additional understanding of the S–R relationship (Table 1).

Table 1. Summary of numerical experiments

Experiments	Horizontal grid size (km)	Emission type
EXP1-R	120	Real (Oliver et al. 1996)
EXP2-R	60	
EXP3-R	20	
EXP4-R	10	
EXP1-C	120	Constant rate
EXP2-C	60	
EXP3-C	20	
EXP4-C	10	

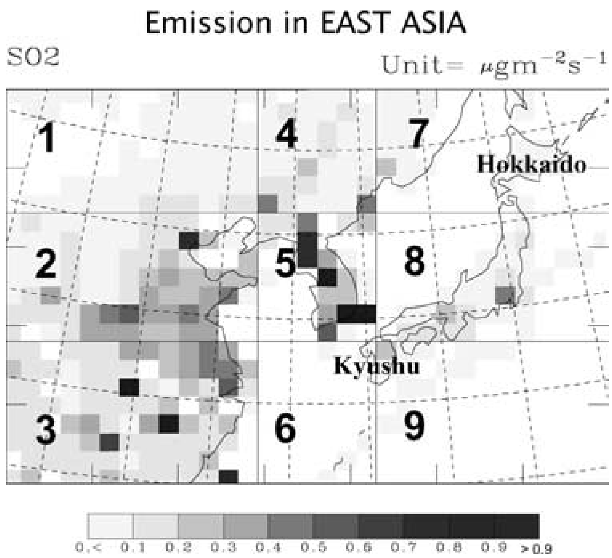

Fig 1. Emission rate for SO_2 (Oliver et al. 1996).

2.2. *Yonsei University's sulfur acid deposition model (YU-SADM)*

YU-SADM considers sulfur components only and has been developed for the evaluation of long-term deposition of sulfur and the S–R relationship. It is one of the participating models in the model intercomparison study for transport and deposition in East Asia (MICS-Asia) (Carmichael et al. 2002). According to the intercomparison study, YU-SADM appears to produce reasonable concentrations and depositions. It produced general features (e.g. location of high concentrations, background values, etc.) that are similar to those of other models, but showed a tendency to produce relatively large peak values of surface SO_2 concentrations and wet sulfate deposition, and relatively sharp spatial concentration gradients.

The governing equation of the gaseous pollutant concentration is given as

$$\frac{\partial C_i}{\partial t} = -\nabla\cdot(C_i\vec{v}) + \nabla\cdot(K_{c_i}\nabla C_i) + R_{c_i} + E_{c_i} + \left(\frac{\partial C_i}{\partial t}\right)_{\text{cloud}} + \left(\frac{\partial C_i}{\partial t}\right)_{\text{dry}} \quad (1)$$

where C_i is the concentration, $\vec{v}$ the wind vector, K_{c_i} the vertical eddy diffusivity, R_{c_i} the chemical transformation rate, E_{c_i} the tendency due to emission, $(\partial C_i/\partial t)_{\text{cloud}}$ the tendency due to wet deposition and $(\partial C_i/\partial t)_{\text{dry}}$ the tendency due to dry deposition.

The model uses polar-stereographic coordinates and terrain-following coordinates for horizontal and vertical directions, respectively. Bott's second-order scheme (Bott 1989, 1992) is used for the calculation of advection. The grid configuration for YU-SADM is the same as that for CSU RAMS.

The profile function type eddy diffusivity of Brost et al. (1988) is used for the vertical diffusion:

$$K_z = kw_*z\left(1 - \frac{z}{z_i}\right) \quad (2)$$

for an unstable planetary boundary layer (PBL),

$$K_z = \frac{ku_*z\,[1-(z/z_i)]^{1.5}}{1+4.7[(z/z_i)(z_i/L)]} \quad (3)$$

for a neutral or stable PBL. Here, k represents the von Karman constant, the height, z_i the PBL depth, w_* the convective velocity scale, u_* the friction velocity and L the Monin–Obukov length. w_* is obtained from the following formula.

$$w_* = \left(\frac{g}{\theta}z_i(\overline{w'\theta'})_0\right)^{1/3}. \quad (4)$$

Surface sensible heat flux, $(\overline{w'\theta'})_0$, is calculated using the method of Louis (1979). The depth of the mixed layer is diagnosed from the profile of potential temperature. Horizontal diffusion is not included.

The following formula used for the MICS-Asia study (Carmichael et al. 2002) is employed here to determine the chemical transformation rate from SO_2 to SO_4:

$$K_c = (1\times10^{-5})\cos\left(1.3\,\text{rlat}\times\frac{\pi}{180}\right) + (4\times10^{-6})\left[1-\cos\left(1.3\,\text{rlat}\times\frac{\pi}{180}\right)\right] \times \sin\left((\text{J}-80)\times2\times\frac{\pi}{365}\right) \quad (5)$$

where rlat is latitude (°N) and J represents the Julian date.

Dry and wet deposition rates are prescribed following the MICS-Asia study (Carmichael et al. 2002). Wet removal rates of SO_2 and sulfate are obtained using the following formulae:

$$D_{SO_2} = (2.0\times10^{-5})\text{Pr}, \quad D_{SO_4} = (5.0\times10^{-5})\text{Pr}^{0.83} \quad (6)$$

where Pr is the precipitation rate (in mm h^{-1}).

Then,

$$\text{WDEP}_{SO_2} = \int_{\tau_{\text{pr}}} C_{SO_2}D_{SO_2}\,\text{d}t \quad (7)$$

$$\text{WDEP}_{SO_4} = \int_{\tau_{\text{pr}}} C_{SO_4}D_{SO_4}\,\text{d}t \quad (8)$$

where WDEP_{SO_2} and WDEP_{SO_4} are the wet deposition amount of SO_2 and SO_4. τ_{pr} represents the duration of precipitation, C_i the vertically integrated concentration of component i for a layer from the surface to the cloud top. The dry deposition velocity is prescribed as a constant depending only on the surface type (land or sea) (Table 2).

2.3. *Calculation of the S–R relationship*

The S–R relationship has been calculated using the following formula:

$$R_{ij} = \frac{H_{ij}}{\Sigma_{i=1}^{n}H_{ij}}\times100(\%) \quad (9)$$

where R_{ij} is the contribution of the ith emission source to the jth receptor and H_{ij} is the deposition amount over the jth receptor when emission is only from the ith source. In this study, the domain is divided into nine S–R regions (Fig. 1).

2.4. *Case*

Numerical experiments are carried out for an episode of extra-tropical cyclone, during which an extra-tropical cyclone propagated eastwards passing the Korean Peninsula and Japan on 17–18 June 1996 (Fig. 2). The cyclone passed the peninsula with a central pressure of 990 hPa around 12:00 UTC on 17 June. The

Table 2. Dry deposition velocity (cm s^{-1})

Species	Land	Sea
SO_2	0.25	0.32
SO_4	0.2	0.1

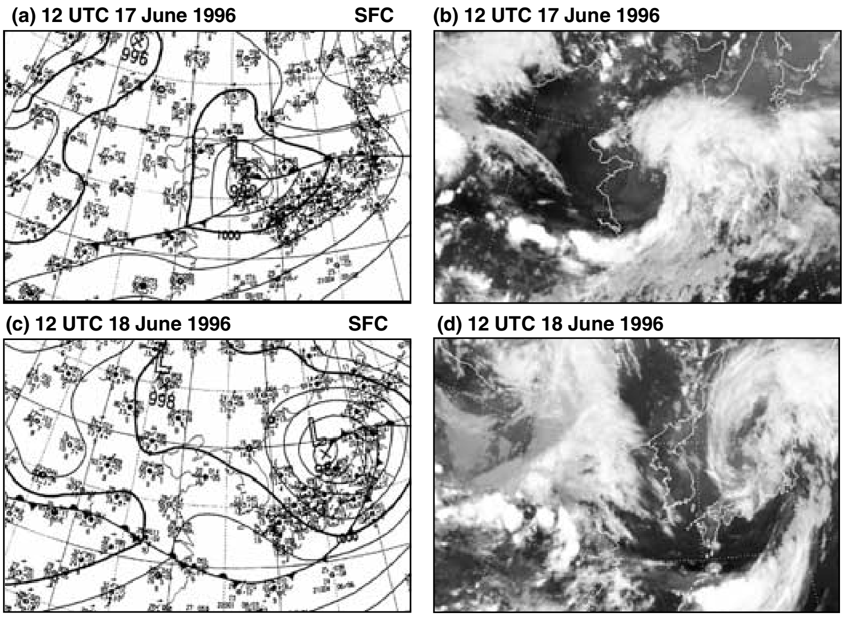

Fig 2. Surface weather charts (left panels, a and c) and satellite images (right panels, b and d).

cold front associated with this cyclone was located between the cyclone centre and the southeastern coast of China near Shanghai. Significant convective clouds were found along the cold front. The cyclone developed further after passing the peninsula and entered the occlusion stage as it passed Japan around 12:00 UTC 18 June 1996. It produced a significant amount of rainfall over the area of its passage.

3. Results

3.1. Simulated meteorological fields

Figure 3 shows the simulated sea-level pressure and cloud fields (integrated condensates amount) for 00:00 UTC on 18 June. The location and intensity of the extra-tropical cyclone varies with the experiment. The deepening of the low is stronger and closer to observations for higher-resolution experiments, although the simulated central pressures are still significantly higher than the observation. The strength of circulation also varies significantly with spatial resolution due to the difference in the deepening. For example, the northerly winds to the west of the Korean Peninsula are much stronger for EXP4 (10 km grid experiment) (Fig. 3i). Simulated cloud fields also show a better agreement with observation for EXP4 than those for lower-resolution experiments. The 10 km grid model has successfully reproduced the clouds associated with the cold front and the occlusion (clouds over the Korean Peninsula).

The simulated fields for 00:00 UTC on 18 June indicate that the development of the simulated cyclone is slower and weaker than the observation, and the location of the cyclone centre is to the south of the observation. At 12:00 UTC on 18 June, however, the results from the 10 km grid model are closer to the observations with an identical central pressure (not shown). The extra-tropical cyclone is weak or does not develop with the 60 and 120 km grids, respectively, while it is as strong as the observed cyclone with the 20 and 10 km grids. However, higher-resolution simulations do not necessarily better reproduce the location of the cyclone centre.

The accumulated rainfall amount for the whole simulation period is shown in Fig. 4. Although the locations of major rainfall areas in the four experiments are somewhat similar to each other, the amount and pattern of rainfall varies greatly with grid size. As the grid size decreases, the amount of rainfall increases significantly in general, especially over the southern half of the Korean Peninsula and Southern Japan, where the cyclone and fronts pass. An extended area of rain is found over the sea between the southeastern coast of China and Southern Japan. It extends further to the east of the Hokkaido Islands. Comparison of the simulated rainfall with the observation over the Korean Peninsula indicates that better agreements are found for the results of the 20 and 10 km grid experiments, although the simulated amount is smaller for all experiments than the observations (not shown).

Figure 5 shows the simulated rainfall amount for the period of 18:00 UTC on 17 June to 06:00 UTC on 18 June, during which the cyclone centre has moved eastwards to the west coast of Central Japan. Thus rainfall has occurred mostly over Japan and the sea to the southwest of Japan. The rainfall over Kyushu and the sea to the southwest of Japan (region 6) is mainly associated with the cold front, while the rainfall over Central Japan (region 8) is mainly due to the precipitation systems over the warm front. Significant differences between the experiments are found in amount of rainfall. Cold frontal rainfall is significant in the simulations with 20 and 10 km grids (EXPs 3 and 4, respectively), but it is not simulated with the 120 and 60 km grids

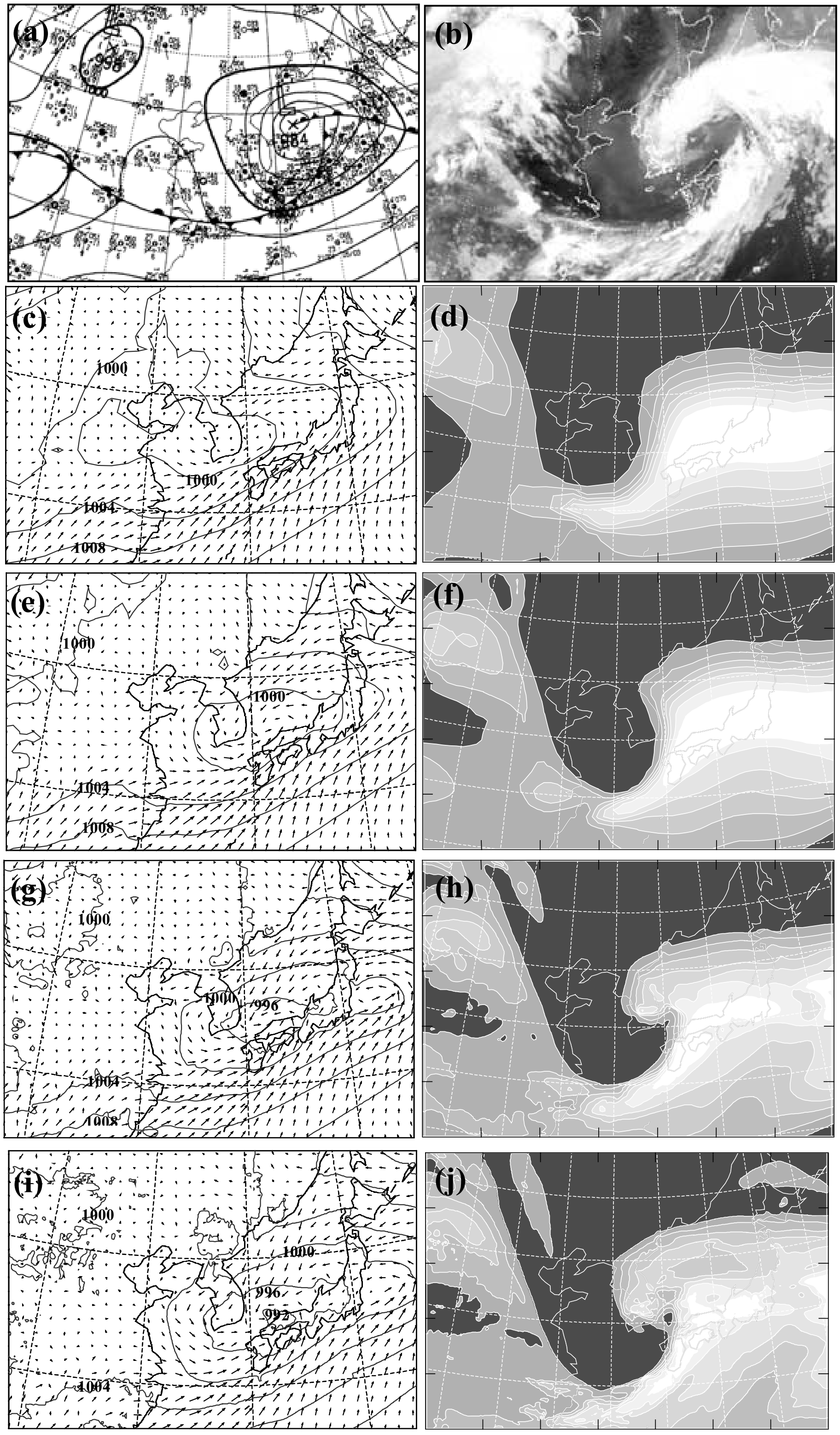

Fig 3. Observed sea-level pressure (SLP) and satellite image for 00:00 UTC on 18 June 1996 (panels a and b, respectively). Simulated fields for SLP (left panels) and vertically integrated amount of condensates (right panels) from EXP1 (c and d), EXP 2(e and f), EXP3 (g and h) and EXP4 (i and j).

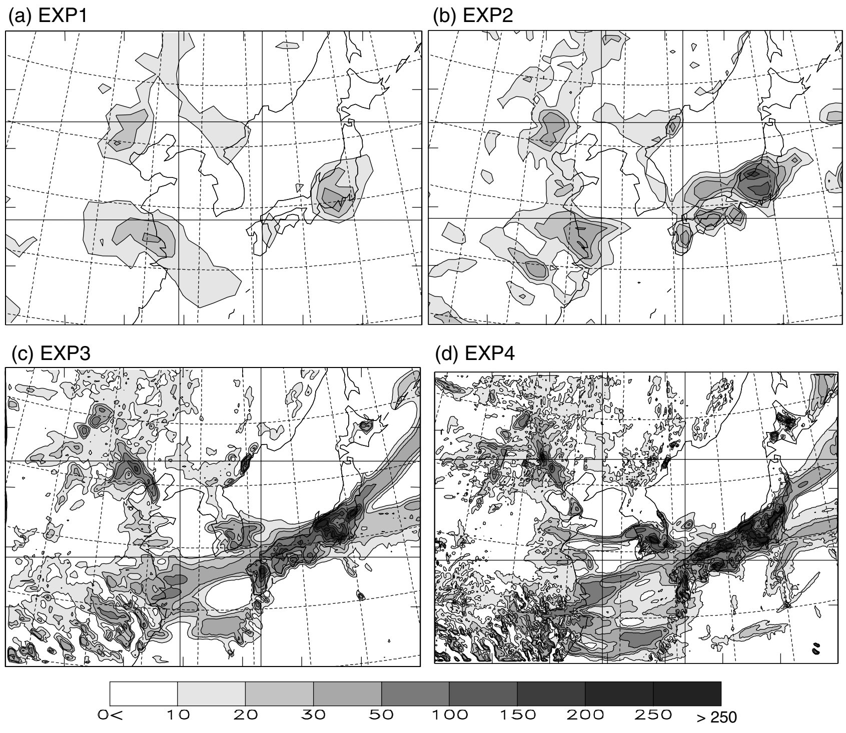

Fig 4. Simulated rainfall amount (mm) for 12:00 UTC 16 June to 12:00 UTC 19 June 1996 from (a) EXP1, (b) EXP2, (c) EXP3 and (d) EXP4.

(EXPs 1 and 2). Warm frontal rainfall is simulated similarly by the experiments except for EXP1, which produces only a small amount of rain over the middle of Japan.

The simulated cyclone appears to be realistic and shows important features of a typical extra-tropical cyclone such as cyclonic circulation, fronts and frontal precipitation, although several inconsistencies are found between the simulation and observations. Enhancement of spatial resolution has improved the simulation, as theory expects. The simulated meteorological fields seem to be adequate for the present study,

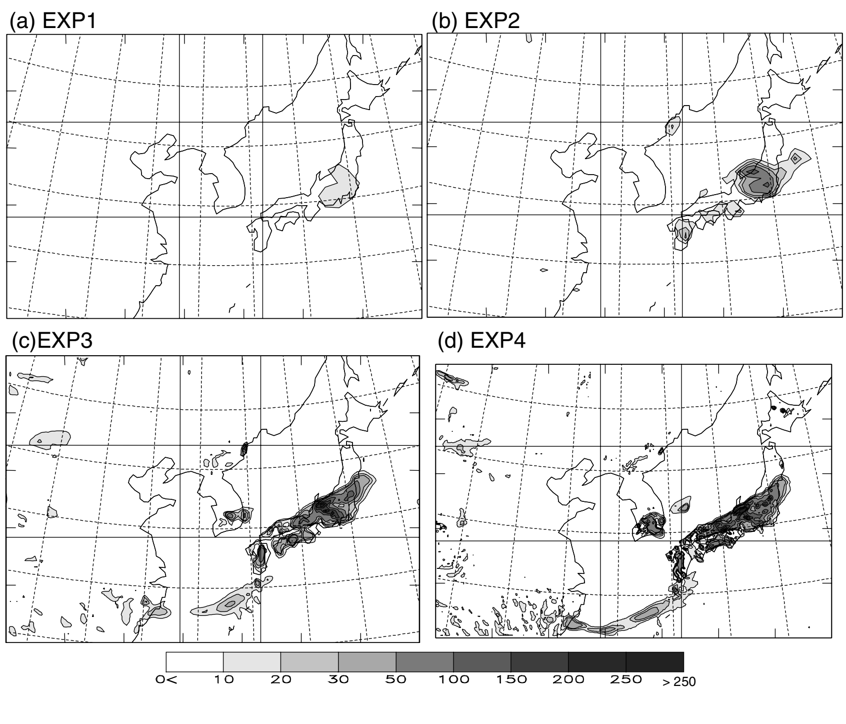

Fig 5. Same as Fig. 4, except for 18:00 UTC 17 June to 06:00 UTC 18 June 1996.

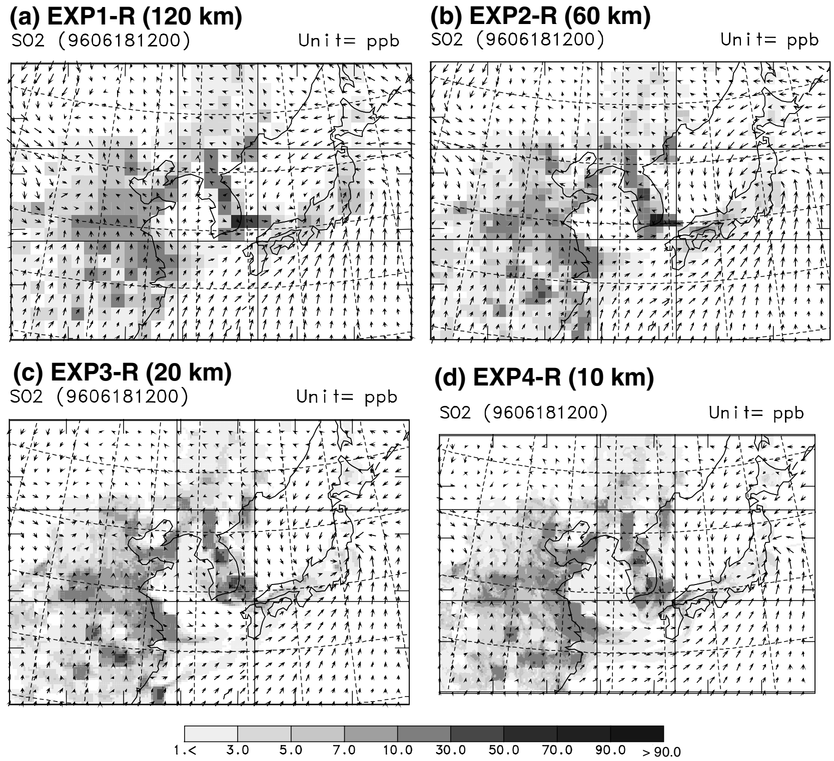

Fig 6. Simulated SO_2 concentration at $z* =$ 48 m from (a) EXP1-R, (b) EXP2-R (c) EXP3-R and (d) EXP4-R for 12:00 UTC on 18 June 1996.

which aims to find out the impact of spatial resolution on the S–R relationship (rather than predicting real-time pollutant fields).

3.2. *Simulated concentration and deposition*

The simulated SO_2 concentration at $z^* = 48$ m is shown in Fig. 6, where z^* is the height in the terrain-following coordinate. All experiments have produced similar concentrations at 12:00 UTC 17 June (not shown). However, some significant differences between the experiments are found in the concentration at 12:00 UTC on 18 June. Surface concentrations over the Korean Peninsula and Japan are smaller for higher-resolution experiments. This may be due to the increased amount of precipitation in these regions for higher-resolution experiments, which enhances the scavenging of locally emitted pollutants. Another important difference is found over the sea to the west and south of the Korean Peninsula. For example, EXP4 shows a significantly higher concentration in these regions than the other experiments in general. This higher concentration can be related to the strength of the simulated cyclone. Stronger winds for EXP4 over the western and southwestern parts of the cyclone induce stronger transport of pollutants from regions 2, 3 and 5 toward region 6 and Southern Japan.

The spatial pattern of amount of dry deposition is similar to those of emission and surface concentration (not shown). Relatively large amounts are found in regions 2, 3 and 5, where emission rates and surface concentrations are relatively large. As found for the surface concentration in Fig. 6, the amount of dry deposition is also somewhat larger for high-resolution simulations over the seas to the west and south of the peninsula. On the other hand, amount of dry deposition over the Korean Peninsula is reduced with enhanced resolution. Otherwise, horizontal grid size does not significantly affect the pattern of dry deposition.

In the case of wet deposition, noticeable differences are found over the area with a large amount of rainfall (e.g. the Korean Peninsula and Southern Japan) (Fig. 7). The amount of wet deposition is significantly larger over those areas for the higher-resolution experiments. A moderate amount of wet deposition due to cold frontal rain in region 6 is represented only for EXPs 3 and 4.

3.3. *Impact of spatial resolution on the S–R relationship*

Dry deposition of sulfur is dominated by self-contribution in most of the regions, except for region 6 where the emission rate is small and the amount of pollutant transported from region 3 is significant (Fig. 8). Relatively large variation of the S–R relationship with spatial resolution is found for regions 6 and 8 where the centre of the low and fronts pass (Figs 8c and d). Region 9, where the emission rate is small, also shows a relatively strong sensitivity to spatial resolution (not shown). In the other

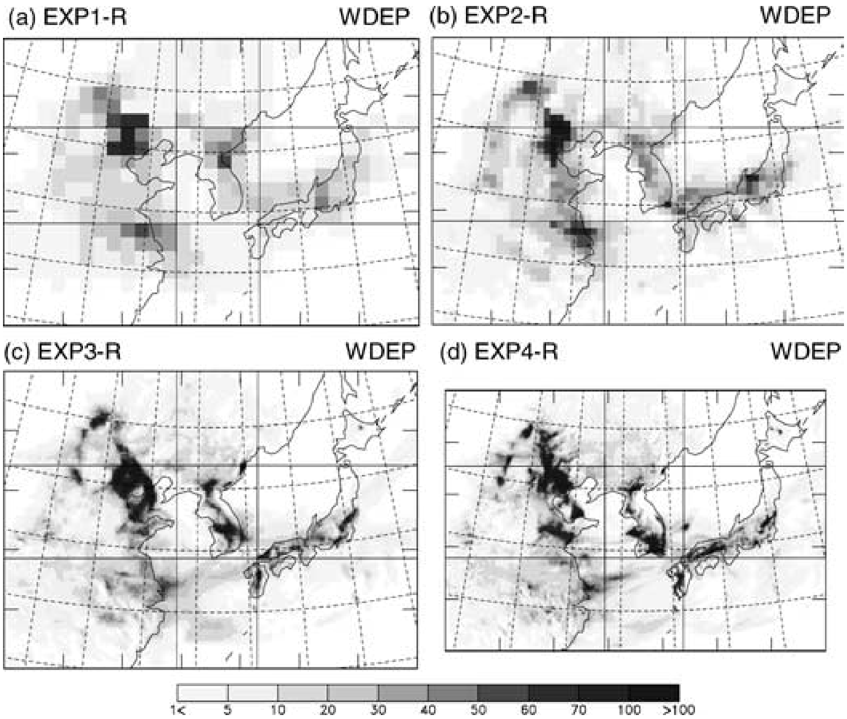

Fig 7. Wet deposition amount (kg km^{-2}) for 12:00 UTC 16 June to 12:00 UTC 19 June 1996 from (a) EXP1-R, (b) EXP2-R, (c) EXP3-R and (d) EXP4-R.

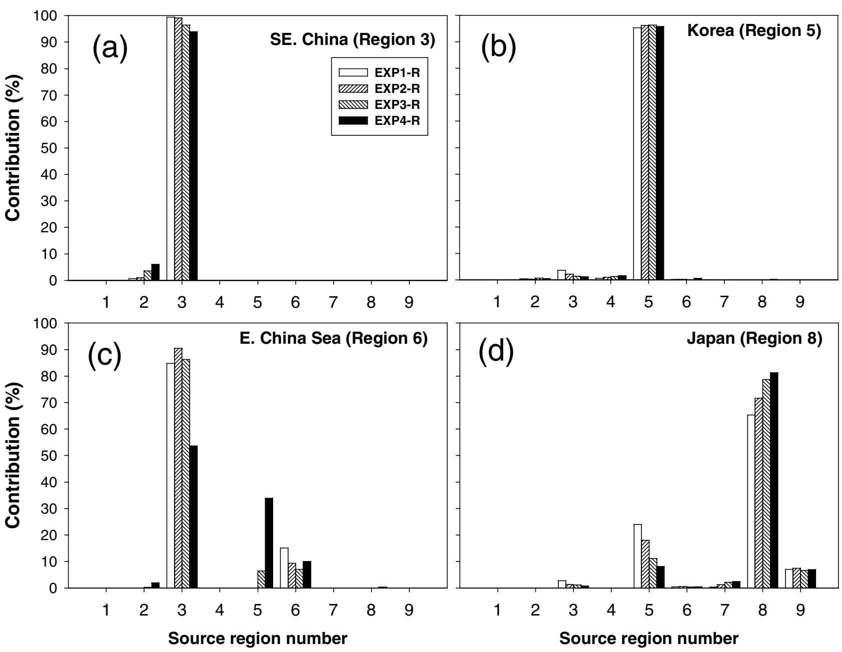

Fig 8. Source–receptor relationship for dry deposition (12:00 UTC 16 June to 12:00 UTC 19 June 1996) in (a) region 3, (b) region 5, (c) region 6 and (d) region 8. Regions are as shown in Fig. 1: 1, Inner and Outer Mongolia; 2, mid-Eastern China; 3, Southeastern China; 4, Northeastern China; 5, Korean Peninsula; 6, East China Sea; 7, Eastern Russia and Northern Japan; 8, Japan; 9, Pacific Ocean.

regions the S–R relationship for dry deposition is not sensitive to the variation of horizontal grid size.

For dry deposition in region 8, the fractional self-contribution increases with increasing spatial resolution, while foreign contributions decrease (Fig. 8d). Note that the fractional contribution of region 5 is significantly smaller for EXP4 than those for low-resolution experiments. This is mainly due to the increased scavenging of pollutants during the transport for EXP4: the average amount of dry deposition in region 8 contributed by region 5 is about 0.52, 0.31, 0.16 and 0.11 kg km^{-2} for 120, 60, 20 and 10 km grid simulations, respectively.

In region 6, where the emission rate is small, self-contribution does not increase with spatial resolution (Fig. 8c). Note that the high-resolution experiments show the contribution of region 5, which is not found for lower resolution. For example, the fractional contribution of region 5 is about 34% for EXP4. On the other hand, the contribution of region 3 has rapidly decreased from about 85–90% for coarse-grid experiments to 53% for EXP4. These changes are mainly due to the increased sulfur transport from region 5 for EXP4. It has been mentioned previously that the strength of circulation, and consequently the pollutant transport toward region 6, is stronger for high-resolution experiments (EXPs 3 and 4). The average amount of dry deposition in region 6 contributed by region 5 is about 0.00, 0.01, 0.11 and 0.41 kg km^{-2} for EXPs 1, 2, 3 and 4, respectively. On the other hand, the amount contributed by region 3 slightly increases from about 0.58 kg km^{-2} for EXP1 to 0.65 kg km^{-2} for EXP4.

The S–R relationship for wet deposition indicates that self-contribution is not as dominant as that for dry deposition, especially in the downstream regions (e.g. regions 6, 7 and 8) (Fig. 9). The relationship varies significantly with spatial resolution in regions 7 and 8. For wet deposition in region 8, the self-contribution increases from less than 20% for EXP1 to about 45% for EXP4, while the contribution from region 3 decreases from 52% for EXP1 to 30% for EXP4. These variations will be explained in greater detail later.

For wet deposition in region 6, where cold frontal rain occurs, contributions from region 5 appear only in EXP3 and EXP4, but their magnitudes are quite small. It is interesting that the contribution from region 5 is negligible or small for wet deposition in region 6, unlike that for dry deposition. This may be explained by a combination of reasons: (1) the amount of wet sulfur deposition is significantly larger than that of dry sulfur deposition in region 6 (1.2 and 9.6 kg km^{-2} for amounts of dry and wet deposition, respectively, for EXP4); (2) sulfur from region 3 dominates the wet deposition in region 6; and (3) air associated with the cold frontal rain is mainly from the warm sector area whose air may have come from the south and southwest (however, in the present case, the sulfur transported at higher levels above the cold front (e.g. 1500 m) seems to be the major contributor to the wet deposition in region 6). This will be discussed further later.

For wet deposition in region 5 (the Korean Peninsula), the S–R relationship is not so sensitive to spatial resolution. In the present simulation, rainfall over the peninsula is produced mainly by

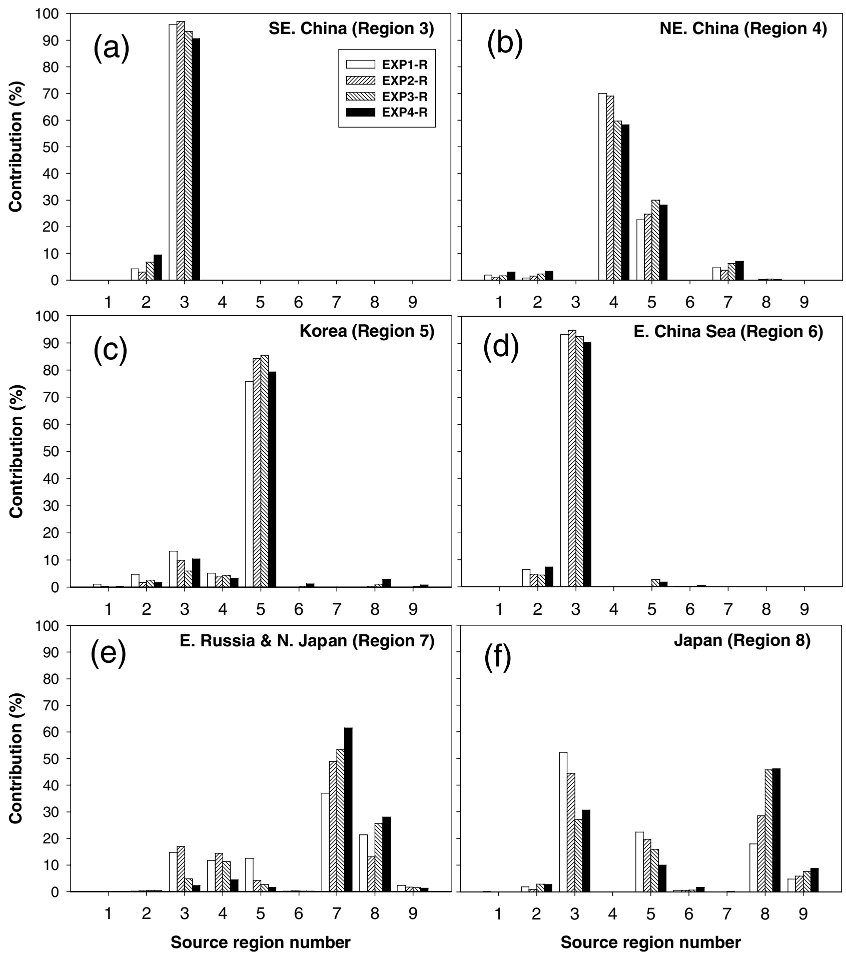

Fig 9. Same as Fig. 8, except for wet deposition in (a) region 3, (b) region 4, (c) region 5, (d) region 6, (e) region 7 and (f) region 8.

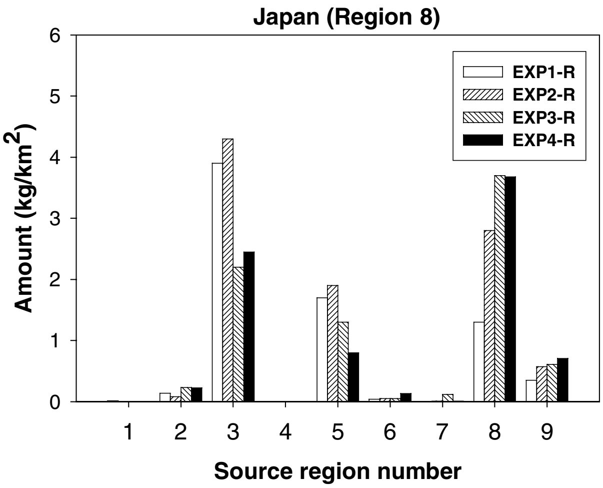

Fig 10. Source–receptor relationship for wet deposition in region 8 during 12:00 UTC 16 June to 12:00 UTC 19 June 1996, in terms of amount of wet deposition (kg km^{-2}) contributed by each region.

precipitation systems in the occlusion area. In region 7, the self-contribution increases with spatial resolution. On the other hand, region 4 shows a decrease in the self-contribution for higher resolution. It is notable that the contribution of region 3 is important in most of its downstream receptor regions (e.g. regions 6, 8 and 9).

The variation of the S–R relationship with spatial resolution is shown again in Fig. 10 for region 8 only, in terms of amount of wet deposition. Its pattern is generally consistent with that in terms of fractional contribution (Fig. 9f). As found in this figure, the increase in the self-contribution with increasing spatial resolution is due to both the increase in wet deposition of locally emitted pollutants and the decrease in deposition of transported pollutants.

Impacts of spatial resolution on the self-contribution can also be described using Fig. 11, which shows area-averaged values of rainfall amount, PBL depth and SO_2 concentrations at $z^* =$ 48 m and 2225 m over region 8. Note that the concentration at 2225 m (Fig. 11d) is the value obtained with emission from region 8 only. This is to show the variation of amount of vertically transported sulfur with spatial resolution. The amount of rainfall increases with increasing spatial resolution, while PBL depth tends to show the opposite variation. The surface concentration also tends to decrease with increasing spatial resolution, even though the PBL depth decreases. This decrease in surface concentration seems due to both increased scavenging and stronger vertical transport of low-level pollutants. The stronger vertical transport can be supported by the larger concentrations for higher resolutions at $z^* = 2225$ m, which is well above the top of the PBL (Fig. 11d). A detailed examination of results has revealed that the larger concentrations at 2225 m for EXPs 3 and 4 are mainly due to stronger convective transport of low-level pollutants (not shown). Consequently, more pollutants become available in EXPs 3 and 4 for scavenging by precipitation throughout convective layers, resulting in increased wet deposition of locally emitted pollutants.

To understand the impact of spatial resolution in a more general sense, the results of experiments with a constant emission rate (for the whole domain regardless of the surface type) were also analysed (not shown). The results indicate that spatial resolution has a small impact on dry deposition in general. For wet deposition, the impact varies with the region. For region 8, where the amount of rainfall is relatively large, enhancing the spatial resolution tends to increase the self-contribution, as already found. However, the magnitude of variability in the S–R relationship is smaller than that for real emission rates. Such weaker impacts with a constant emission rate may be explained by the fact that the transported component occupies a relatively small portion of the total amount of deposition in a certain receptor region. This suggests that the relatively large impact of spatial resolution found for real emission experiments is due to the large difference in the amount of pollutant emission between the regions (e.g. regions 3 and 8), implying that the impacts are exaggerated to some extent in regions with relatively small emission.

The present study has shown that enhancement of spatial resolution tends to increase the self-contribution but to decrease foreign contributions to the wet deposition in receptors located in the path of an extra-tropical cyclone. It has been found that enhanced scavenging due to increased precipitation, for higher spatial resolution, reduces the amount of transported pollutants but increases the deposition of locally emitted pollutants. The increase in the self-contribution for higher resolution may also be partially due to the enhanced strength of resolved convection. The impact of enhancing spatial resolution on dry deposition is felt mostly over downstream regions (regions 6, 8 and 9). Contributions of upstream sources increase as cyclonic circulation becomes stronger with increasing spatial resolution.

3.4. *The S–R relationship for wet deposition in an extra-tropical cyclone*

Wet deposition associated with an extra-tropical cyclone occurs mainly in the warm and cold frontal areas. During the present episode, the simulated cyclone fully develops as it approaches the Japanese Islands and exhibits some typical features of an extra-tropical cyclone such as the fronts, frontal rain, three-dimensional circulation, occlusion, etc. Thus, the S–R relationship derived for the period of cyclone passage may give us some insight into the typical relationship for wet deposition associated with an extra-tropical cyclone, which is a very important agent for wet deposition of transported pollutants in mid-latitude regions.

To show the S–R relationship for wet deposition associated with the present cyclone, additional calculations have been

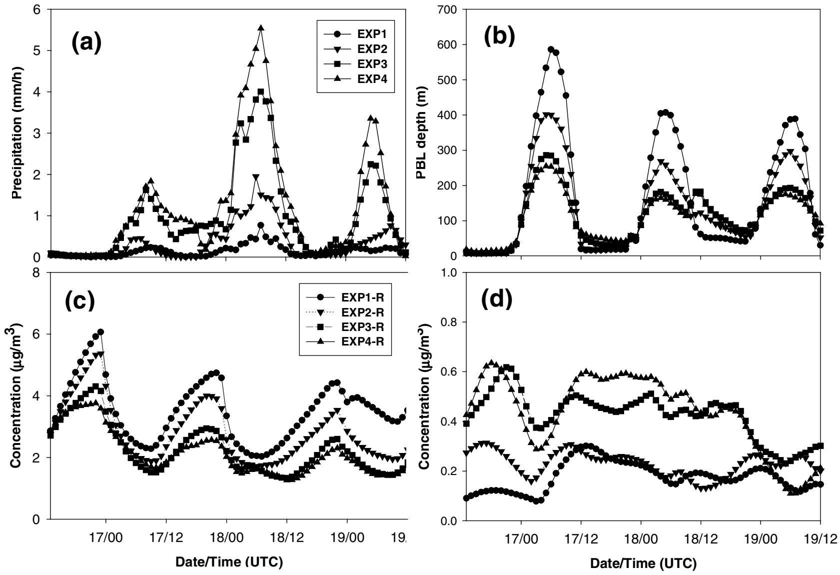

Fig 11. Temporal variation of area-averaged fields over region 8 for (a) amount of precipitation, (b) PBL depth, and SO_2 concentration at (c) $z^* = 48$ m, and (d) $z^* = 2225$ m.

carried out for particular periods: 18:00 UTC on 17 June to 00:00 UTC on 18 June for warm frontal rain and 18:00 UTC on 17 June to 06:00 UTC on 18 June for cold frontal rain. Significant warm frontal rain occurs over the middle of Japan (Region 8) and cold frontal rainfall over the sea to the south of Korea (Region 6) during the respective rainfall periods. The reason for a shorter period (6 h) for warm frontal rain is to avoid the mixing of cold and warm frontal rain in region 8 caused by the eastward movement of the cyclone. The calculation has been carried out for both occasions of real and constant emission rates, using the 10 km grid meteorological data.

In region 6, where cold frontal rain has occurred, wet deposition is dominated by the contribution of region 3 when the real emission rate is used (Fig. 12a). The dominance seems to be due to the fact that region 6 is the downstream neighbour of region 3 and also due to the large contrast in amount of emission between the two regions. Air from region 3 is flowing into both the warm sector area and the northern side of the cold front. When a constant emission rate is used, the self-contribution is about 31% and the rest of the wet deposition is mostly due to region 3. Note that the contribution of region 5, which is not negligible for dry deposition (see Fig. 8c), is negligible for wet deposition in region 6, as also found in Fig. 9d.

The large contribution of region 3 to the wet deposition in region 6, for the period of 18:00 UTC on 17 June to 06:00 UTC on 18 June, may be explained in the following manner. Sulfur concentration over the warm sector area is small in this case. Thus, it is unlikely that sulfur from the warm sector region is responsible for the major portion of deposited sulfur. Examination indicates that a significant portion of the pollutants deposited in the cold frontal rain area have been transported at higher levels above the cold front (e.g. 1500 m). The pollutants appear to be transported upward in source regions by turbulent mixing during the daytime and by convection, and then horizontally transported at higher levels. As they arrive at the cold frontal area, they become involved in wet deposition.

For wet deposition in region 8, where warm frontal rain has occurred, the fractional contributions of region 8 itself and region 3 are about 18% and 68%, respectively, when real emission is used (Fig. 12b). The rest of the wet deposition is due

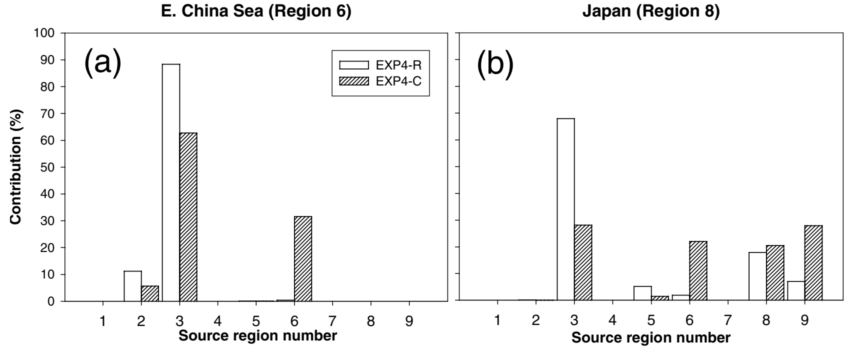

Fig 12. Source–receptor relationship for the wet deposition in (a) region 6 (East China Sea) during 18:00 UTC 17 June to 06:00 UTC 18 June (cold frontal rain period) and (b) region 8 (Japan) during 18:00 UTC 17 June to 00:00 UTC 18 June (warm frontal rain period).

to regions 5, 6 and 9. When a constant emission rate is used, the fractional self-contribution does not change much from that with real emission, but foreign contributions are quite different from those with the real emission. The contributions of regions 3, 6 and 9 are comparable to each other. Note that these regions are located to the southwest, south and southeast of the cyclone centre, respectively.

The present results indicate that the sources of pollutants deposited by warm frontal rain are the receptor region itself and the regions located to the southern side of the cyclone track. The sources of pollutants in cold frontal rain include the receptor and the southwestern region. Thus the major sources for wet deposition within an extra-tropical cyclone are the receptor region itself and the source regions on the southern side of the cyclone, especially the southwestern source. In this case, pollutants from southeastern China contribute the most to the wet deposition associated with the cold and warm frontal rainfalls. On the other hand, the sources on the northern side of the cyclone do not contribute much to the wet deposition within the cyclone. This seems understandable when we consider the typical circulation of an extra-tropical cyclone. Within a typical extra-tropical cyclone, the low-level air over the northern side of the front is trapped under cold and warm frontal surfaces, while the low-level air over the warm sector area flows toward the frontal surfaces, producing rain. Recent trajectories of the low-level air in the warm sector area are likely from the south and southwest of the cyclone centre. Thus the sources in the northern side of a cyclone are less likely to be important contributors to wet deposition in an extra-tropical cyclone.

4. Summary and conclusions

A numerical study has been made to evaluate the impact of horizontal grid size on the estimation of the S–R relationship. Numerical experiments with four different horizontal grid sizes have been performed for an extra-tropical cyclone episode. CSU RAMS and YU-SADM (the Yonsei University sulfur acid deposition model) have been used to simulate meteorological and pollutant fields, respectively.

In this study, enhanced spatial resolution has improved the simulation of an extra-tropical cyclone, a cold front and its associated precipitation systems. As spatial resolution increases, the circulations associated with the cyclone and cold front become stronger, and the amount of frontal rainfall increases.

This study indicates that enhancement of spatial resolution tends to increase the self-contribution but decrease foreign contributions to the wet deposition associated with an extra-tropical cyclone. It has been found that increased precipitation for enhanced spatial resolution reduces the amount of transported pollutant, but increases the wet deposition of locally emitted pollutants. The larger self-contribution for higher resolution may also be partially due to the increased strength of resolved convection. The impact of enhancing spatial resolution on dry deposition is felt mostly over downstream regions (regions 6, 8 and 9) where the centre of the low and the fronts pass. Contributions of upstream sources increase as cyclonic circulation becomes stronger with increasing spatial resolution.

On the other hand, enhancing the spatial resolution does not significantly affect the S–R relationship for either dry or wet deposition in the other regions where the extra-tropical cyclone does not pass. This study indicates that the improved simulation of the cold front does not significantly affect the S–R relationship for wet deposition over the area of passage of the cold front. This study also indicates that the impacts of spatial resolution can be exaggerated for receptors with relatively small emission.

The present study has shown that the major sources for the wet deposition associated with cold and warm frontal rainfalls are the regions on the southern side of the extra-tropical cyclone. On the contrary, the sources on the northern side do not contribute much to the wet deposition. In the present case, pollutants from southeastern China make the biggest contribution to the wet deposition in the downstream receptors.

According to this study, the variation of the derived S–R relationship with spatial resolution is caused by variations in the amount of precipitation and circulation strength. Since the pattern and magnitude of these variations can vary significantly with model and case, the generality of the present conclusions is yet to be proved through more studies using different models and cases.

5. Acknowledgments

This research has been supported by the Korea Ministry of Science and Technology through the National Research Laboratory Program. The authors wish to thank anonymous reviewers for their valuable comments.

References

Arndt, R. L., Carmichael, G. R. and Roords, J. M. 1998. Seasonal source–receptor relationships in Asia. *Atmos. Environ.* **31**, 1553–1572.

Bott, A. 1989. A positive definite advection scheme obtained by nonlinear renormalization of the advective fluxes. *Mon. Weather Rev.* **117**, 1006–1015.

Bott, A. 1992. Monotone flux limitation in the area-preserving flux-form advection algorithm. *Mon. Weather Rev.* **120**, 2592–2602.

Brost, R. A., Haagenson, P. L. and Kuo, Y.-H. 1988. The effect of diffusion on tracer puffs simulated by a regional scale Eulerian model. *J. Geophys. Res.* **93**(D3), 2389–2404.

Calori, G., Carmichael, G. R., Streets, D., Thongboonchoo, N. and Guttikunda, S. K. 2001. Interannual variability in sulfur deposition in Asia. *J. Global Environ. Eng.* **7**, 1–16.

Carmichael, G. R., Hayami, H., Calori, G., Uno, I., Cho, S. Y. et al. 2002. The MICS-Asia study: model intercomparison study of long range transport and sulfur deposition in East Asia. *Atmos. Environ.* **36**, 175–199.

Huang, M., Wang, Z., He, D., Xu, H. and Zhou, L. 1995. Modeling studies on sulfur deposition and transport in East Asia. *Water, Air, and Soil Pollution* **85**, 1927–1932.

Ichikawa, Y. and Fujita, S. 1995. An analysis of wet deposition of sulfate using a trajectory model for East Asia. *Water, Air, and Soil Pollution* **85**, 1921–1926.

Louis, J.F., 1979. A parametric model of vertical eddy fluxes in the atmosphere. *Bound.-Layer Meteor.* **17**, 187–202.

Oliver, J. G. J., Bouwman, A. F., van der Maas, C. W. W., Berdowski, J. M., Veldt, C. et al. 1996. Descriptions of EDGAR Version 2.0: a set of global emission inventories of greenhouse gases and ozone depleting substances for all anthropogenic and most natural sources on a per country basis and on $1^\circ \times 1^\circ$ grid. *National Institute of Public Health and the Environment (RIVM) Report* 77 1060 002/TNO-MEP no R96/119, RIVM, Bilthoven, Netherlands. 141 pp.

Pielke, R. A., Cotton, W. R., Walko, R. L., Trembeck, C. J., Nicholls, M. E. et al. 1992. A comprehensive meteorological modeling system—RAMS. *Meteorol. Atmos. Phys.* **49**, 69–91.